ACS APPLIED MATERIALS & INTERFACES

Research Article

www.acsami.org

Biaxially Mechanical Tuning of 2-D Reversible and Irreversible Surface Topologies through Simultaneous and Sequential Wrinkling

Jie Yin,[†,⊥] Jose Luis Yagüe,[‡,⊥] Mary C. Boyce,*[,§,∥] and Karen K. Gleason*[,‡]

[†]Department of Mechanical Engineering, Temple University, Philadelphia, Pennsylvania 19122, United States

[‡]Department of Chemical Engineering and [§]Department of Mechanical Engineering, Massachusetts Institute of Technology, Cambridge, Massachusetts 02139, United States

[∥]Department of Mechanical Engineering, Columbia University, New York, New York 10027, United States

Supporting Information

ABSTRACT: Controlled buckling is a facile means of structuring surfaces. The resulting ordered wrinkling topologies provide surface properties and features desired for multifunctional applications. Here, we study the biaxially dynamic tuning of two-dimensional wrinkled micropatterns under cyclic mechanical stretching/releasing/restretching simultaneously or sequentially. A biaxially prestretched PDMS substrate is coated with a stiff polymer deposited by initiated chemical vapor deposition (iCVD). Applying a mechanical release/restretch cycle in two directions loaded simultaneously or sequentially to the wrinkled system results in a variety of dynamic and tunable wrinkled geometries, the evolution of which is investigated using in situ optical profilometry, numerical simulations, and theoretical modeling. Results show that restretching ordered herringbone micropatterns, created through sequential release of biaxial prestrain, leads to reversible and repeatable surface topography. The initial flat surface and the same wrinkled herringbone pattern are obtained alternatively after cyclic release/restretch processes, owing to the highly ordered structure leaving no avenue for trapping irregular topological regions during cycling as further evidenced by the uniformity of strains distributions and negligible residual strain. Conversely, restretching disordered labyrinth micropatterns created through simultaneous release shows an irreversible surface topology whether after sequential or simultaneous restretching due to creation of irregular surface topologies with regions of highly concentrated strain upon formation of the labyrinth which then lead to residual strains and trapped topologies upon cycling; furthermore, these trapped topologies depend upon the subsequent strain histories as well as the cycle. The disordered labyrinth pattern varies after each cyclic release/restretch process, presenting residual shallow patterns instead of achieving a flat state. The ability to dynamically tune the highly ordered herringbone patterning through mechanical stretching or other actuation makes these wrinkles excellent candidates for tunable multifunctional surfaces properties such as reflectivity, friction, anisotropic liquid flow or boundary layer control.

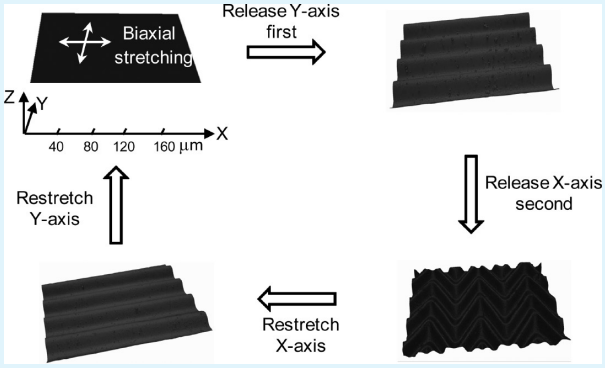

KEYWORDS: *buckling, chemical vapor deposition, computer modeling, pattern, thin films*

INTRODUCTION

Wrinkled surfaces obtained through buckling of a stiff coating on a compliant substrate have found applications in a wide variety of areas, including stretchable electronics,[1] thin film properties measurement,[2] photovoltaics,[3] microfluidics,[4] adhesion,[5,6] wetting,[4,7] fouling/antifouling systems,[8,9] cell culture biointerfaces,[10] and so forth. Upon mismatched mechanical,[7] thermal,[11] or swelling[12] deformation in the bilayer system, uniaxial or biaxial compressive stress is developed in the coating, which spontaneously leads to various one-dimensional (1-D)[11,13−15] or two-dimensional (2-D)[4,16,17] wrinkling patterns after buckling. The mechanism of wrinkling instability in soft composite materials has been extensively studied through experimental and theoretical approaches, which was thoroughly discussed in several recent review papers.[18−20]

Compared to wrinkling induced by isotropic thermal or swelling strain, mechanical stretching provides greater independent control of application and release of strains in two directions, which allows dynamic manipulation of wrinkling and wrinkled patterns through mechanical strain tuning. Without requiring traditionally lithographic tools and masks, the dynamic tuning of wrinkling patterns via mechanical strain offers a cost-effective and reliable method for rapidly generating tunable ordered micropatterned surfaces over large area as well as their related active control of surface related properties. Recently Yang et al.[7] studied the reversible and dynamically

Received: November 27, 2013
Accepted: February 3, 2014
Published: February 3, 2014

   dx.doi.org/10.1021/am4054207 | ACS Appl. Mater. Interfaces 2014, 6, 2850−2857

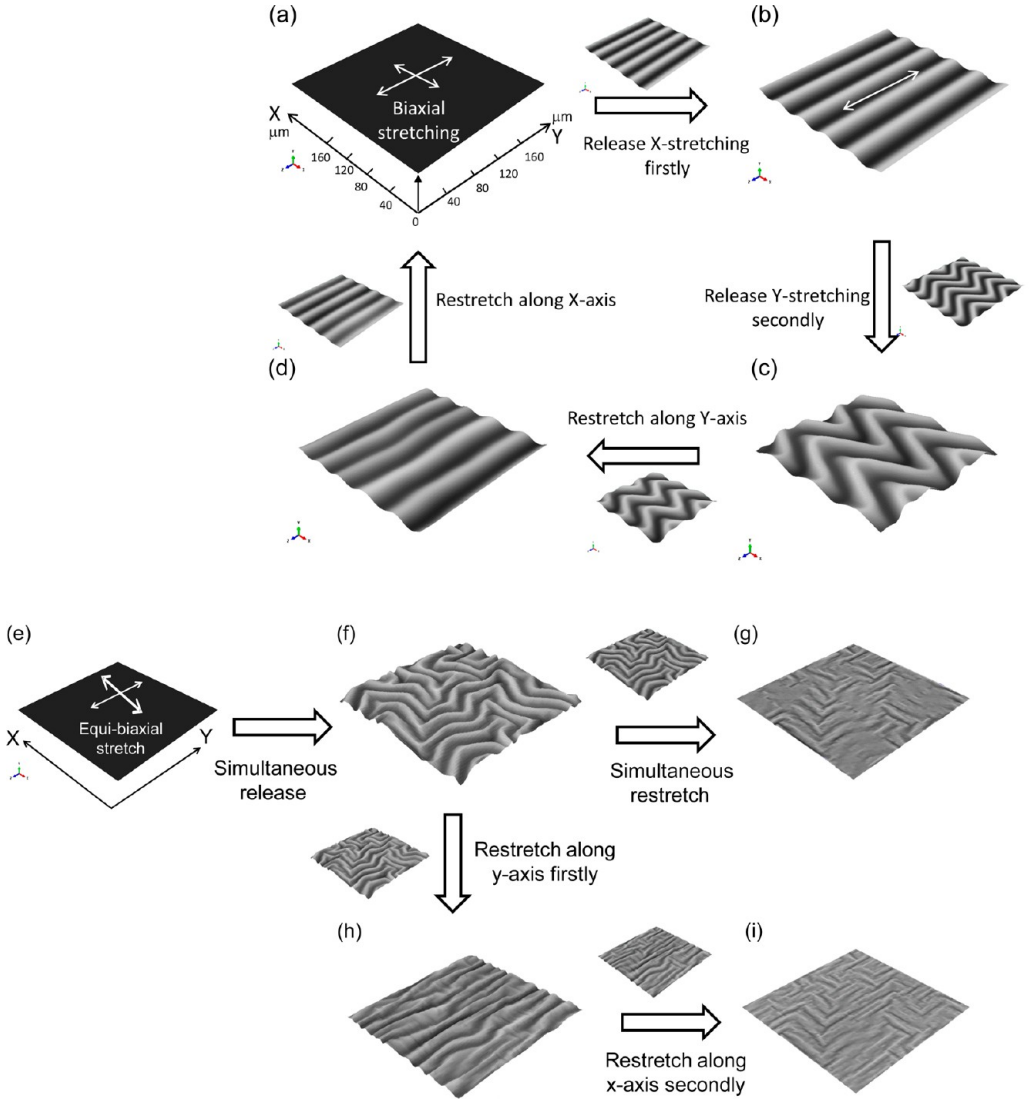

Figure 1. FEM simulation of the dynamic tuning of wrinkling patterns produced through strain releasing and reloading: (a−d) reversible ordered patterns after sequential release and restretch; (e−i) irreversible disordered patterns after simultaneous and sequential restretch. (a) A stress-free p(EGDA) polymer thin coating is deposited on a biaxially stretched PDMS (not shown in figure), (b) first release of strain along *x*-axis leads to 1D wrinkles; (c) sequential release of strain along the *y*-axis results in 2-D zigzag herringbone patterns; (d) 2-D wrinkles transit to 1-D wrinkles upon restretching along the *y*-axis and finally become nonwrinkled flat surface after stretching along the *x*-axis; (e) simultaneous release of equi-biaxial stretched PDMS leads to 2-D labyrinth patterns (f); (g) residual pattern after simultaneous restretching labyrinth pattern (f) to its original strain; (h) wrinkling pattern after restretching labyrinth pattern along the *y*-axis first; (i) residual pattern after restretching along the *x*-axis second.

tunable surface topography of 1-D wrinkles through mechanical releasing and restretching, which has found wide applications in tunable adhesives, dynamic switching of wetting surface, and tunable open-channel microfluidics. Ohzono and Monobe[21] investigated the dynamic shape-tunability and reversible response of microwrinkles by applying additional compressive strains, where they demonstrate the controllability of periodicity and ordering of complex wrinkling patterns, as well as their novel applications in liquid manipulation and repeatedly switchable alignment of liquid crystals.

However, most previous studies have focused on the dynamic tunable and reversible surface topography of either 1-D sinusoidal wrinkles or 2-D complex wrinkle stripe patterns when subjected to uniaxial restretching or compression. Compared to the uniaxial mechanical strain, biaxial strain provides more options for dynamic tuning of 2-D surface morphology through simultaneous or sequential releasing-restretching cycles, which still remains unexplored. In addition, the loading history dependent or independent 2-D wrinkling pattern is unknown when biaxially mechanical restretching is applied. The ability to actively reconfigure the two-dimensionally patterned geometrical features on the surface would be a key enabler for many new applications, including reflectivity, wettability, microfluidic flow, and boundary layer control, and photovoltaic.[22]

In this paper, based on our recent research on the creation of deterministic ordered 2-D herringbone surface patterns through sequential wrinkling,[17] the surface evolution of both ordered 2-D herringbone patterns and disordered labyrinth pattern under sequentially or simultaneously dynamic release (unloading) and restretch (reloading) in two directions is studied using both experimental and finite element method simulation approaches. The dynamic tuning of wrinkling patterns in response to controlled loading and unloading is analyzed using in situ three-

dx.doi.org/10.1021/am4054207 | ACS Appl. Mater. Interfaces 2014, 6, 2850−2857

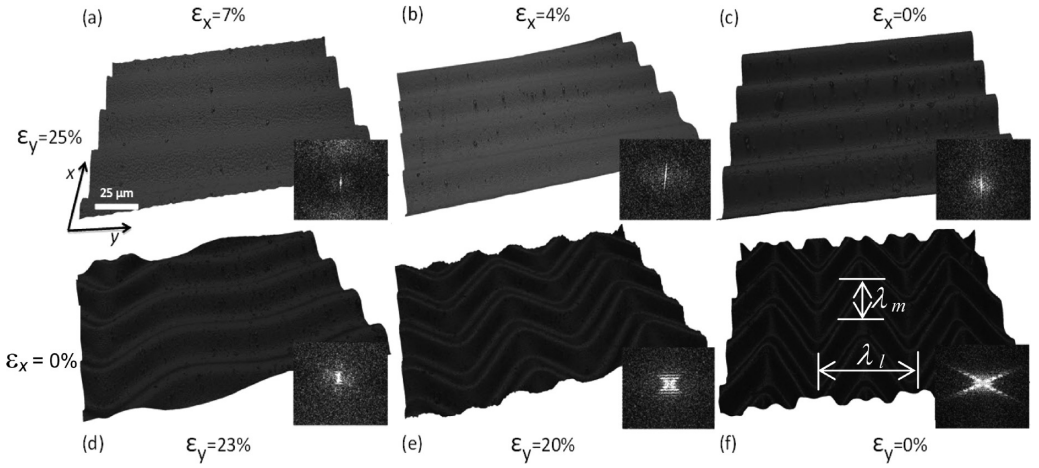

Figure 2. Wrinkling patterns of EGDA coating on PDMS substrates upon sequential release of biaxial strains with a prestrain of 10% along *x*-axis and a prestrain of 25% along *y*-axis. Panels (a) to (c) correspond to strain release along the *x*-axis, and from (d) to (f) to strain release along the *y*-axis. The scale bar (25 μm) applies to all images. The inset graphs show the Fourier transform image analysis of the samples.

dimensional (3-D) optical profilometry and compared with simulated and analytical results. The dynamic unloading and reloading processes of biaxial strains are schematically illustrated in Figure 1 for both ordered herringbone patterns and disordered labyrinth patterns. A thin poly(ethylene glycol diacrylate) (p(EGDA)) film is deposited on a biaxially prestretched PDMS substrate (Figure 1a) using iCVD, a solvent-free technique that yields conformal and functional polymer thin films.[13,14] During the unloading process, the biaxially prestretched strain is sequentially released in the *x* and the *y* direction (Figure 1b and c) to yield ordered herringbone zigzag wrinkling patterns. The composite substrate/coating system with ordered wrinkled surface patterns is then reloaded by restretching to the same prestrain in the two directions sequentially (Figure 1d). Restretching causes the disappearance of the wrinkles, and hence demonstrates the reversibility of ordered patterns during cyclic loading/unloading. However, simultaneous release of equi-biaxially prestretched strain yields disordered labyrinth patterns (Figure 1e and f). When such disordered patterns are then either simultaneously (Figure 1g) or sequentially (Figure 1h and i) reloaded by restretching to the initial biaxial prestrain, a residual shallow wrinkled patterns remains in the surface, showing the irreversibility of disordered patterns (Figure 1f and i).

EXPERIMENTAL SECTION

Substrate Preparation. The PDMS substrate is prepared through several steps. The PDMS was synthesized using the Sylgard 184 Silicone Elastomer Kit from Dow Corning. The elastomer and the curing agent were thoroughly mixed at a mass ratio of 10:1 and poured into Petri dishes with a PDMS layer of about 2 mm. The Petri dishes were put in a vacuum desiccator for degasification for 90 min and then cured in an oven at 70 °C for 2 h. Cruciform-shaped PDMS films 6 cm long with a central square region of 2 cm × 2 cm were cut using an Epilog laser cutter for the experiments.

Pattern Formation. The samples were placed in a custom-built sample holder with a screw driven stretching mechanism, compatible with the iCVD reactor, for biaxial stretching. The cruciform tab regions of the PDMS sample were gripped between jaws and biaxially stretched to a specific elongation. After the p(EGDA) deposition on PDMS, samples were subjected to either simultaneous or sequential quasi-static release. The release rate was approximately 10 $\mu m \cdot s^{-1}$.

iCVD Polymerization. A layer of trichlorovinylsilane (97%, Sigma) was used as an adhesion promoter between PDMS and p(EGDA). First, the PDMS surface was activated using a plasma oxygen treatment in a plasma cleaner (Harrick Scientific PDC-32G) at 18 W for 30 s. Immediately, the biaxially stretched cruciform-shaped PDMS film was introduced in an oven at 40 °C under vacuum and exposed to trichlorovinylsilane vapors for 5 min. Next, the PDMS sample was placed into a custom-built cylindrical reactor (diameter 24.6 cm and height 3.8 cm) to conduct the iCVD polymerizations. EGDA (98%, PolySciences) was heated to 60 °C and was introduced into the reactor at a flow rate of 0.5 sccm by using a regulated needle valve. *tert*-Butyl peroxide (TBPO) (98%, Aldrich) was fed into the chamber at a flow rate of 1.5 sccm through a mass flow controller (MKS Instruments). ChromAlloy filaments (Goodfellow) were resistively heated to 230 °C. The distance between the filaments and the stage was kept at 2 cm. The stage was back-cooled by water using a chiller/heater (Neslab RTE-7) and the temperature was set at 25 °C. Polymer thickness was monitored in situ by laser interferometry (JDS Uniphase).

Dynamic Pattern Characterization. The dynamic evolution of the surface pattern and its features were analyzed with a 3-D optical profilometer (Zeta-20, Zeta Instruments) at different steps of the release and restretch process.

Simulation Details. The simulation is based on the finite element method (FEM) and conducted using the commercial software ABAQUS. The coating is modeled as a linear, isotropic and elastic material with the measured Young's modulus of E_f = 775 ± 30 MPa and a Poisson's ratio $\nu_f \approx 0.4$ of a self-standing EGDA film. The PDMS substrate is a nonlinear elastic elastomeric material and modeled as a hyperelastic almost incompressible Neo-Hookean material with measured Young's modulus E_s = 0.45 ± 0.02 MPa and Poisson's ratio ν_s = 0.49. The material properties characterization of both EGDA coating and PDMS are described in ref 17. For more details of simulation, please refer to ref 17.

RESULTS AND DISCUSSION

Reversible Ordered Herringbone Wrinkled Pattern after Restretching. Figure 2 displays the formation process of a typical herringbone wrinkling pattern upon the sequential release of a biaxially stretched sample along two directions, where the PDMS is prestretched to a strain of 10% along the *x*-direction and 25% along the *y*-direction and then coated with p(EGDA) to a coating thickness of 400 nm. Upon first release of the prestrain of 10% along the *x*-axis, the coating is under uniaxial compression and leads to the first formation of 1-D sinusoidal wrinkling pattern (Figure 2a–c), where its amplitude increases and wrinkling wavelength decreases with increasing released strain. Upon second release of the prestrain of 25%

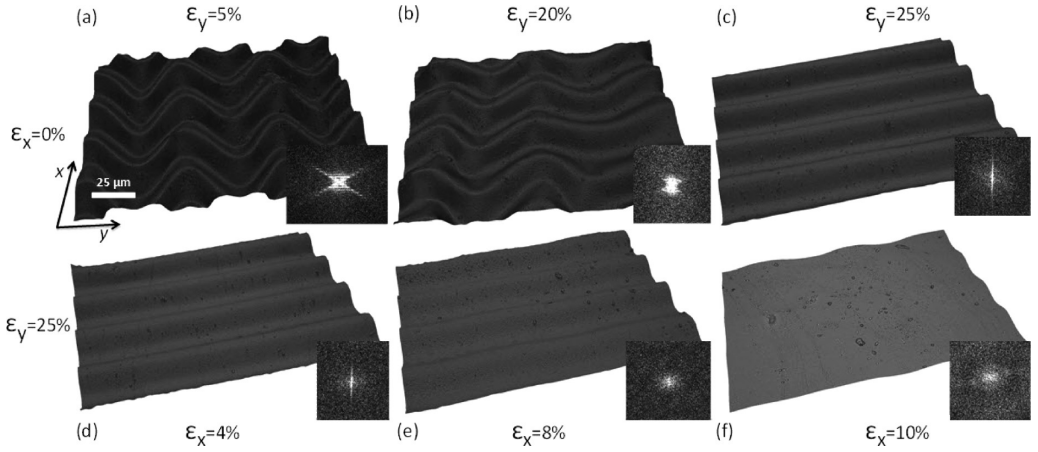

Figure 3. Evolution of wrinkling patterns through sequential restretching of wrinkled EGDA coating on PDMS substrates along two directions to the original stretching strain of 10% along the *x*-axis and 25% along the *y*-axis. Panels (a) to (c) correspond to restretch in the *y*-axis, and panels (d) to (f) correspond to the *x*-axis. The scale bar (25 μm) applies to all images. The inset graphs show the Fourier transform image analysis of the samples.

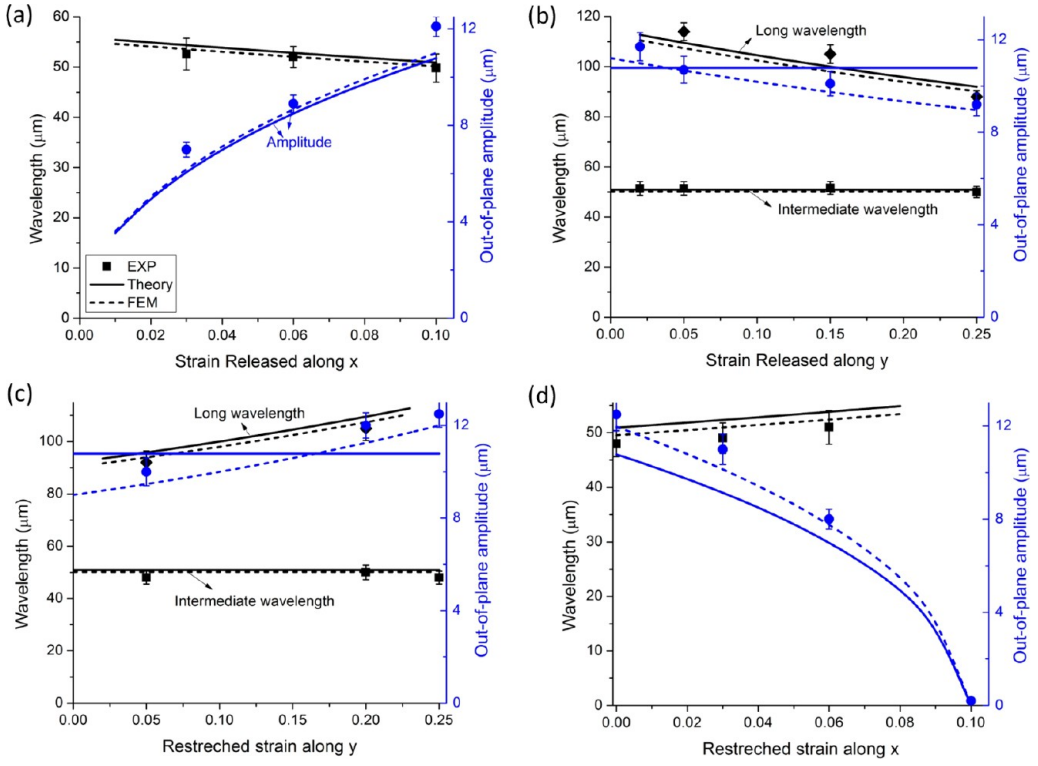

Figure 4. Comparison of wrinkle wavelength and amplitude between experiments (data points), FEM simulation (dashed lines), and analytical models (solid lines) upon sequential releasing and reloading of biaxial strain.

along the *y*-axis, the 1-D sinusoidal wrinkles are subjected to the compression along the *y*-direction, which leads to buckling of 1-D sinusoidal columns along the *x*-direction and thus a 2-D zigzag herringbone pattern is formed. The geometry of herringbone structures can be characterized by the zigzag turning angle, that is, jog angle (α), and the intermediate (λ_m) and long wavelengths (λ_l). λ_m and λ_l are the distance between two adjacent jogs in the *y*-axis and *x*-axis as demonstrated in Figure 2f. As shown in Figure 2e and f, λ_l decreases from 114 to 88 μm and α decreases from 100° to 62°. In contrast, λ_m, which is equal to the wavelength λ in the 1-D wrinkle, remains constant at 50 μm. The shortening of λ_l stems from the increasing compressive stress along the *y*-axis in the coating. The out-of-plane amplitude *A* (along *z*-axis) decreases from 12 to 9 μm.

The quantitative amplitude information provided by optical profilometry enables computation of the 2-D Fourier transform (FT), which is given in an inset for each sample in Figure 2 to show the evolution and periodicity over the entire sample area (600 μm × 600 μm). The white spots correspond to the frequency of the wave and its harmonics. Therefore, for 1-D patterns (Figure 2a–c), the frequency is displayed vertically, indicating the periodicity along one direction. During release of the *y*-axis strain, FT images show the transition from a vertical lined pattern to an X-shaped pattern (Figure 2e and f), which demonstrates a periodicity in two directions and reflects the zigzag pattern feature. Additionally, the cross angle of the X-

dx.doi.org/10.1021/am4054207 | ACS Appl. Mater. Interfaces 2014, 6, 2850–2857

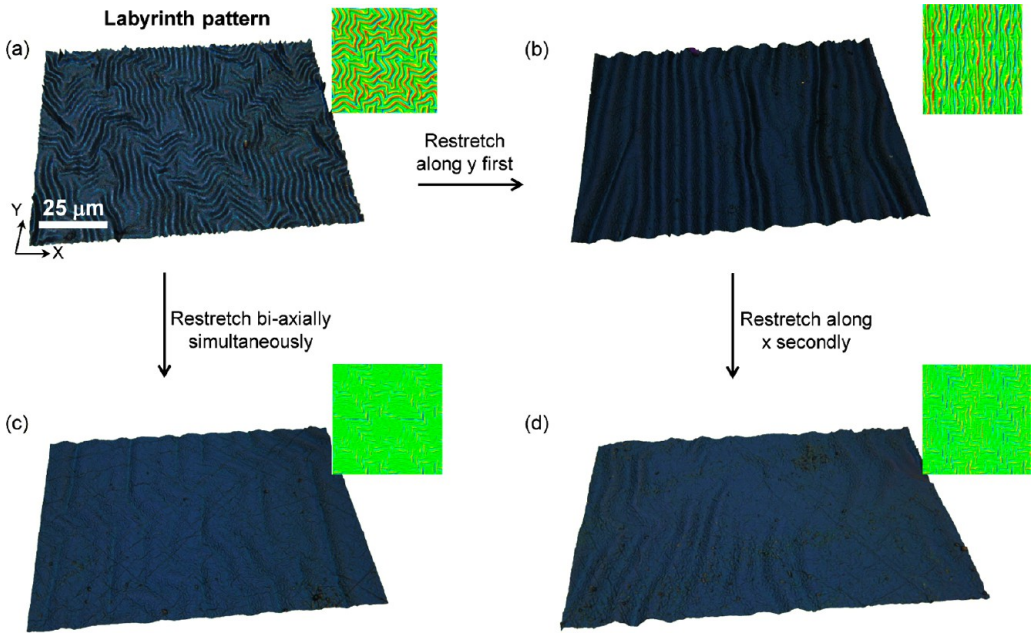

Figure 5. Evolution of wrinkling patterns after either sequential or simultaneous restretch of a labyrinth pattern in the EGDA coating on PDMS; small icon figures show the corresponding simulated displacement contours along the *z*-axis using FEM: (a) chaotic pattern created upon simultaneous release of equi-biaixal strain of 5% along the *x*- and *y*-axis direction; (b) intermediate pattern after first restretched strain of 5% along the *y*-axis; (c) residual pattern after simultaneous biaxial restretch of 5%; (d) residual pattern after second restretched strain of 5% along the *x*-axis direction. The scale bar (25 μm) applies to all images.

shape reflects the jog angle of the zigzag herringbone pattern. As the strain released in the *y*-axis increases, the cross angle of the X-shape decreases from above to below 90°, agreeing with the experimentally observed surface topography. Increasing the area from which optical profilometry data can be obtained would enable even more FT detailed analysis, as the degree of order in the patterns should be reflected in the sharpness of the transform peaks. At the current maximum analysis size, the dominate source of peak broaden occurs as a result of the assumption of periodic boundary conditions rather than the disorder of the pattern itself.

The reversibility of the 2-D zigzag herringbone pattern under biaxial restretching is examined next. The pattern is sequentially restretched to its initial state with first a 25% strain along the *y*-direction and then a 10% strain along the *x*-direction (Figure 3). It should be noted that the reversibility is retained when changing the sequence of the biaxial restretching, which is discussed in Figure S1 in the Supporting Information. Generally, the pattern evolution during the restretching is reverse to that observed during the strain releasing, where a 2-D herringbone pattern gradually transits to a 1-D sinusoidal pattern after restretching alongthe *y*-direction (Figure 3a–c). Upon a subsequent restretching along the *x*-direction, the 1-D pattern goes back to a nearly flat surface without any residual pattern (Figure 3d–f), which indicates the reversibility of the 2-D herringbone pattern after a nonequi-biaxial releasing-restretching process.

Figure 3a–c shows the transition from the 2-D wrinkled pattern to the 1-D pattern upon restretching along the *y*-axis to a strain of 25%. The measurement of the wrinkle wavelength and amplitude shows that λ_m remains almost constant with a value of around 50 μm, while the amplitude *A* increases from 9 to 12 μm (Figure 4c). The wrinkle geometry is almost the same as that observed in the release process, indicating a reversible evolution in topography during unloading and reloading of the same strain. Furthermore, after restretching along *x*-axis to its original strain of 10% (Figure 3d–f), amplitude *A* of the sinusoidal wrinkle decreases (Figure 4d) until no evidence of wrinkles is observed on the coating surface (Figure 3f). FT image evolution is seen to follow the same sequence during restretching as observed during release. Thus, sequential release allows different patterns to be achieved simply by tuning the stretch and/or release of the mechanical strain applied.

Additionally, after another cycle of release/restretch, the flat surface transits into the same herringbone pattern as shown in Figure S2 in the Supporting Information. As proved in ref 17, a herringbone pattern created through sequential release of biaxial prestrain possesses the minimum strain energy and thus both deterministic short and long wavelength. The deterministic nature of the wrinkle formation during sequential release enables this reversibility since the deterministic wrinkling wavelength and amplitude are only dependent on material properties and applied strains.

The evolution of wrinkling patterns during the strain releasing and restretching is simulated using the FEM method and also analytically modeled, which provides a quantitative manipulation tool on dynamically tuning the geometry of wrinkling patterns. Figure 1 shows the evolution of simulated reversible wrinkling patterns from flat surface to 2-D zigzag morphology upon unloading and reloading, which agrees well with the experimental observations (Figures 2 and 3). Quantitative comparisons of simulation and experimental wrinkle wavelengths and amplitudes were studied in more detail.

The wrinkle wavelength and amplitude are determined by the material properties of the polymer coating and the PDMS substrate, the coating thickness, and the magnitude and history of the biaxial prestrain. When considering the finite deformation in the coating for relatively large stretching, during the release of the first strain (ε^{1st}), 1-D sinusoidal

wrinkles are formed, and are characterized by a wavelength (λ) and an amplitude (A) given by[15]

$$\lambda = \frac{2\pi t(\bar{E}_f/3\bar{E}_s)^{1/3}}{1+\varepsilon^{1st}}, \quad A = \frac{t\sqrt{\varepsilon^{1st}/\varepsilon_{cr}-1}}{\sqrt{1+\varepsilon^{1st}}} \tag{1}$$

where t is the coating thickness, $\bar{E}$ is $E/(1-\upsilon^2)$ with E being the Young's modulus and υ being the Poisson ratio, and subscripts s and f refer to substrate and film, respectively. From eq 1, it can be seen that when the prestrain ε^{1st} is much less than 1, eq 1 will reduce to the classical buckling wavelength and amplitude of 1-D wrinkles.[23,24] The critical buckling strain (ε_{cr}) $\varepsilon_{cr} = -(3\bar{E}_s/\bar{E}_f)^{2/3}/4$, for the p(EGDA)-PDMS system, was found to be 0.37%. For the 2-D zigzag herringbone pattern upon release of the second strain (ε^{2nd}), the intermediate wavelength (λ_m), long wavelength (λ_l), and amplitude (A') are calculated based on the model in Yin et al.[17]

$$\lambda_m = \lambda, \quad \lambda_l = 2.06\pi t(1-\nu_f^2)^{1/4}\left(\frac{\bar{E}_f}{3\bar{E}_s}\right)^{1/2}\frac{1}{1+\varepsilon^{2nd}},$$
$$A' = A \tag{2}$$

where λ_m and A' are equal to the wrinkle wavelength λ and amplitude A of the 1-D wrinkles in eq 1, respectively. Equations 1 and 2 also work for the corresponding wavelength and amplitude upon restretching of wrinkles.

Figure 4 shows the comparison of amplitude and wavelengths obtained during the release and restretch process using analytical models (eqs 1 and 2), FEM simulations and experiments. For both 1-D and 2-D wrinkles formed during the release and restretch of the strain, the corresponding wavelengths obtained from theoretical models agree well with experiments. For 2-D wrinkles obtained at small strains, theoretical models predict a constant value of the amplitude. However, during the release of a relatively large strain (i.e., 25%) along y-axis, the amplitude decreases slightly with the increasing strain released. This tendency is observed in both experiments and simulations (Figure 4b and c).

Irreversible Disordered Labyrinth Pattern after Restretching. Unlike the reversible nature of ordered herringbone pattern after cyclic release/restretch, a disordered labyrinth pattern surface morphology shows its irreversible characteristics after either sequential or simultaneous restretching (Figure 5). Figure 5a shows a labyrinth wrinkle pattern of a 200 nm thick EGDA coating with out-of-plane wrinkle amplitude of 8.2 μm, which is obtained upon simultaneous release of an equi-biaxial prestrain of 5%. After sequentially restretching this wrinkled EGDA-PDMS composite system to the same 5% strain in two directions, a residual zigzag pattern is found exhibiting a small out-of-plane amplitude of about 720 ± 42 nm (Figure 5c). During the sequential restretching of the biaxial strain, the ordering of the disordered labyrinth pattern occurs after the first restretching of 5% strain along the y-axis, where the orientation for most of the wrinkles is along y-direction (Figure 5b). Similar ordering of such complex wrinkling patterns into 1-D striped patterns is also observed under additional compressive strains on Pt-coated PDMS systems.[25] Furthermore, the surface exhibits a 1-D wrinkled pattern with dislocation-like defects in the form of branched wrinkles (Figure 5b). Most of the 1-D wrinkles are not straight but exhibits a slight bend laterally along the x-direction. Such dislocation-like defects and lateral bending play an important role in the irreversible process, where strain energy is highly concentrated in the location of defects and lateral bending points, which may act as "singularity" points of the strain energy. Upon a second restretching along the x-direction, such defects migrates but are not annihilated, where most of the strain energy in the coatings are released but with some strain energy remained in the locations with defects (see the FEM simulation discussed later). Another reason for the residual pattern may arise from the plastic deformation in the stress concentrated defect locations. During simultaneous biaxial restretching of labyrinth patterns, the out-of-plane amplitude of labyrinth patterns decreases and similar shallow zigzag pattern remains with amplitude of about 810 nm after simultaneous restretching to the same 5% in two directions (Figure 5d) due to the similar dislocation defect behavior or possible plastic deformation.

Furthermore, when the residual shallow pattern is subjected to another sequential release of the equi-biaxial strain, the residual shallow pattern is surprisingly found to transit to a different labyrinth pattern from its original one (Figure S3a, Supporting Information). Theoretically, an ordered wrinkled herringbone pattern is favorable to be formed after sequential release of stretch. However, despite its small amplitude, the residual pattern following the simultaneous unloading may serve as an initial defect structure and have a large influence on the resulting pattern after buckling together with possible plastic deformation. Similarly, upon simultaneous release of restretching in the composite system with the residual shallow pattern, similar labyrinth pattern is observed (Figure S3b, Supporting Information).

Corresponding FEM simulations are also carried out to investigate the surface topography evolution of a labyrinth pattern during its restretching (inset of Figure 5). In confirmation with our experimental observations, irreversible characteristics of a labyrinth pattern remain after either simultaneous or sequential restretching (Figure 5c and d). Especially interesting is the fact that, after the first sequential stretching, the labyrinth pattern transits to a 1-D wrinkled pattern with several dislocation-like defects (Figure 5b). The strain energy remaining in the film upon simultaneous release is ~2% of the energy stored in the original labyrinth pattern and about 3% after sequentially restretching (Figure S4, Supporting Information). Thus, these defects can act as a local energy minimum where the pattern is trapped, demonstrating that the final configuration depends on the loading/unloading history. During the simultaneous restretch, simulation shows that the labyrinth pattern is preserved while its out-of-plane amplitude continuously decreases. When the chaotic pattern is restretched to the initial value of 5%, it transits to a shallow zigzag pattern, which shows a short wavelength equal to the one in the labyrinth pattern. During the sequential restretch, a defect-riddled 1-D wrinkled pattern emerges after the first release of strain in the y-axis as shown in the inset of Figure 5b, which agrees with the experimental observation.

Discussion on Residual and Reversible Pattern during Cyclic Loading/Unloading: Insights from Simulation. The labyrinth wrinkled pattern exhibits a random orientation of jogs and wrinkles, where the orientation of some jogs is nearly aligned with either the x- or the y-axis while others show randomly inclined orientation (see top-right corner of Figure 5a). After simultaneous or sequential restretching, residual wrinkle/jog patterns are observed which depend on the simultaneous vs sequential nature of the restretching history. These patterns are essentially topologically "trapped in"

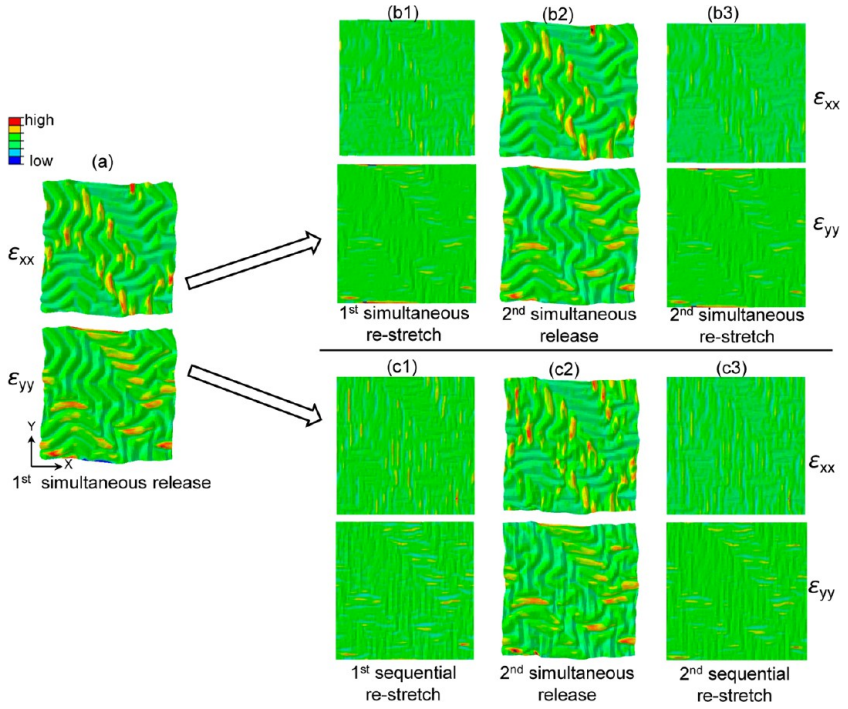

Figure 6. Simulated normal strain contours along *x* and *y*-axis on the top layer of PDMS substrate during cyclic simultaneous release/restretch of equi-biaxial strain of 5%: (a), (b1), (b2), and (b3) show a two-cycle simultaneous release/simultaneous restretch; (a), (c1), (c2), and (c3) show a two-cycle simultaneous release/sequential restretch.

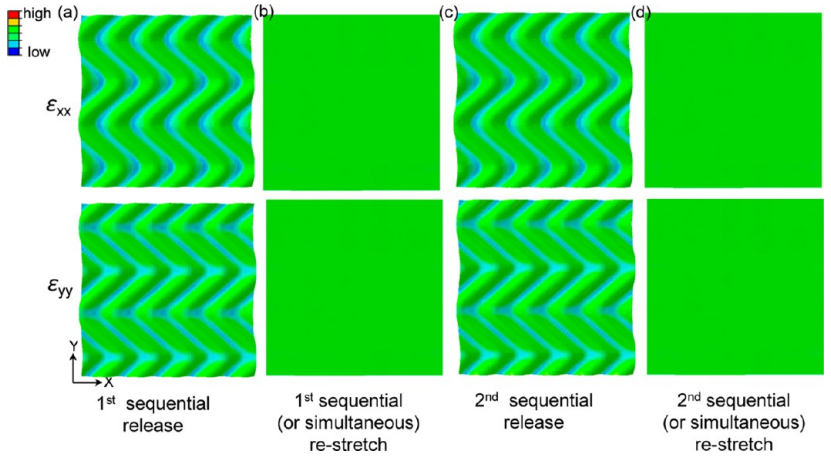

Figure 7. Simulated normal strain contours along *x*- and *y*-axis on the top layer of PDMS substrate during cyclic sequential release/restretch of equi-biaxial strain of 5%: all panels show a two-cycle sequential release/sequential (or simultaneous) restretch.

depending upon the loading history and can also be observed be examining the strain distribution in the substrate. A closer examination of the in plane normal strain evolution on the surface of the substrate during loading/reloading in FEM simulations is conducted to shed light on the irreversible and reversible pattern formation.

Figure 6 shows the simulated contours of normal strain along the *x*- (ε_{xx}) and *y*-axis (ε_{yy}) on the substrate surface during a two-cycle history of simultaneous release followed by either simultaneous or sequential restretching. We first observe that the labyrinth pattern (Figure 6a) exhibits heterogeneously distributed regions of strain with regions of very high strain concentration particularly in the irregular jog topology regions. Upon restretching, residual strains are observed and found to depend upon the restretching history; these residual strains also depend on the number of cycles. The irregular topology/high strain concentration regions act to alter the manner in which topologies can form in subsequent cycles since they essentially act as defects which guide the formation of the next topology. We further note that the simulations are elastic and yet still exhibit residual strains and topologies, further highlighting the trapped topology mechanism; any plasticity that is likely to be occurring would further interfere with reversibility.

In contrast to the labyrinth patterns, the herringbone patterns show a highly ordered wrinkle/jog pattern and highly uniform strain, leaving no avenues for trapping in residual topologies. Figure 7 shows the simulated contours of normal strain ε_{xx} and ε_{yy} on the surface of the substrate during a two-cycle sequential release/simultaneous (or sequential) restretch, where the reversibility and reproducibility of herringbone

dx.doi.org/10.1021/am4054207 | ACS Appl. Mater. Interfaces 2014, 6, 2850−2857

pattern and flat surface are well demonstrated and consistent with the experimental observation. In contrast to the regions of highly concentrated strain in the labyrinth pattern (Figure 6), the ordered herringbone patterns show a uniform strain distribution in its zigzag jogs along both x and y axis followed by a near zero residual strain and flat surface during the cycling off and hence reversible topology upon cycling and release.

CONCLUSION

In summary, this study shows the ability to use strain histories to dynamically tune the surface microtopography of 2-D deterministic herringbone and disordered labyrinth patterns obtained via buckling mechanism. Herringbone patterns produced by sequential loading histories are reversible during cyclic mechanical stretching/releasing/restretching processes, while labyrinth patterns produced by simultaneous release result in nonreversible patterns during subsequent cyclic loading histories. The labyrinth leads to local topological regions which are highly strained and disordered which, in turn, lead to trapped topological zones and residual strain upon cycling. These trapped topological zones influence the wrinkle/jog pattern formation in subsequent cycling and hence the irreversibility of labyrinth pattern formation. Ordered herringbone patterns, created through sequential release, provide a highly ordered topology with no regions of high strain concentration, which leaves no avenue for topology trapping during cycling and hence provides for reversibility. Restretching such a 2-D ordered herringbone wrinkling pattern transits to a flat surface without any residual topology pattern or strain. Cyclic releasing−restretching−releasing process in this system always drives to the same herringbone pattern configuration demonstrating the repeatability and reversibility of the process and the herringbone patterns. The agreement between simulation, theoretical modeling, and experiments confirms the reproducibility of the process and can help to quantitatively design the desired surface on demand. FT analysis of the images has been used to study the ordering of the pattern. Ordered patterns show frequencies following the periodicity of the sample.

The possibility to reversibly modify the topography by applying strain can provide a means to yield surfaces with tunable functionality. Mechanical strain or other actuation can be used to dynamically tune the pattern and its corresponding surface properties actively during use. For example, reversible wrinkled to flat surfaces could be used to provide bonding or adhesion with quick-release capability, or to actively alter a surface's reflectivity, wettability, microfluidic flow, or boundary layer control.

ASSOCIATED CONTENT

Supporting Information

Figures of ordered and disordered wrinkling patterns after cyclic loading/unloading. This material is available free of charge via the Internet at http://pubs.acs.org.

AUTHOR INFORMATION

Corresponding Authors

*E-mail: mcboyce@mit.edu.
*E-mail: kkg@mit.edu.

Author Contributions

⊥J.Y. and J.L.Y. contributed equally to the paper.

Notes

The authors declare no competing financial interest.

ACKNOWLEDGMENTS

The authors thank the King Fahd University of Petroleum and Minerals in Dharan, Saudi Arabia, for funding the research under the Grant No. 016403-011 reported in this paper through the Center for Clean Water and Clean Energy at MIT and KFUPM.

REFERENCES

(1) Rogers, J. A.; Someya, T.; Huang, Y. *Science* **2010**, *327*, 1603−1607.
(2) Chung, J. Y.; Nolte, A. J.; Stafford, C. M. *Adv. Mater.* **2011**, *23*, 349−368.
(3) Kim, J. B.; Kim, P.; Pegard, N. C.; Oh, S. J.; Kagan, C. R.; Fleischer, J. W.; Stone, H. A.; Loo, Y. L. *Nat. Photonics* **2012**, *6*, 327−332.
(4) Ohzono, T.; Monobe, H.; Shiokawa, K.; Fujiwara, M.; Shimizu, Y. *Soft Matter* **2009**, *5*, 4658−4664.
(5) Chung, J. Y.; Youngblood, J. P.; Stafford, C. M. *Soft Matter* **2007**, *3*, 1163−1169.
(6) Yoo, P. J.; Lee, H. H. *Langmuir* **2008**, *24*, 6897−6902.
(7) Yang, S.; Khare, K.; Lin, P.-C. *Adv. Funct. Mater.* **2010**, *20*, 2550−2564.
(8) Efimenko, K.; Finlay, J.; Callow, M. E.; Callow, J. A.; Genzer, J. *ACS Appl. Mater. Interfaces* **2009**, *1*, 1031−1040.
(9) Shivapooja, P.; Wang, Q.; Orihuela, B.; Rittschof, D.; López, G. P.; Zhao, X. *Adv. Mater.* **2013**, *25*, 1430−1434.
(10) Greco, F.; Fujie, T.; Ricotti, L.; Taccola, S.; Mazzolai, B.; Mattoli, V. *ACS Appl. Mater. Interfaces* **2012**, *5*, 573−584.
(11) Bowden, N.; Brittain, S.; Evans, A. G.; Hutchinson, J. W.; Whitesides, G. M. *Nature* **1998**, *393*, 146−149.
(12) Breid, D.; Crosby, A. J. *Soft Matter* **2011**, *7*, 4490−4496.
(13) Basu, S. K.; Scriven, L. E.; Francis, L. F.; McCormick, A. V. *Prog. Org. Coat.* **2005**, *53*, 1−16.
(14) Chung, J. Y.; Chastek, T. Q.; Fasolka, M. J.; Ro, H. W.; Stafford, C. M. *ACS Nano* **2009**, *3*, 844−852.
(15) Jiang, H. Q.; Khang, D. Y.; Song, J. Z.; Sun, Y. G.; Huang, Y. G.; Rogers, J. A. *Proc. Natl. Acad. Sci. U.S.A.* **2007**, *104*, 15607−15612.
(16) Cavicchi, A.; Gambarotta, L.; Massabò, R. *Finite Elem. Anal. Des.* **2009**, *45*, 519−529.
(17) Yin, J.; Yagüe, J. L.; Eggenspieler, D.; Gleason, K. K.; Boyce, M. C. *Adv. Mater.* **2012**, *24*, 5441−5446.
(18) Li, B.; Cao, Y.-P.; Feng, X.-Q.; Gao, H. *Soft Matter* **2012**, *8*, 5728−5745.
(19) Singamaneni, S.; Tsukruk, V. V. *Soft Matter* **2010**, *6*, 5681−5692.
(20) Chen, X.; Yin, J. *Soft Matter* **2010**, *6*, 5667−5680.
(21) Ohzono, T.; Monobe, H. *J. Colloid Interface Sci.* **2012**, *368*, 1−8.
(22) Lipomi, D. J.; Chong, H.; Vosgueritchian, M.; Mei, J.; Bao, Z. *Sol. Energy Mater. Sol. Cells* **2012**, *107*, 355−365.
(23) Huang, Z. Y.; Hong, W.; Suo, Z. *J. Mech. Phys. Solids* **2005**, *53*, 2101−2118.
(24) Chen, X.; Hutchinson, J. W. *J. Appl. Mech.* **2004**, *71*, 597−603.
(25) Ohzono, T.; Shimomura, M. *Phys. Rev. B* **2004**, *69*, 132202.